

**One-step femtosecond laser patterning of light-trapping structure on dye-sensitized solar cell photoelectrode**

Journal:	<i>Journal of Materials Chemistry C</i>
Manuscript ID:	TC-ART-11-2014-002657.R1
Article Type:	Paper
Date Submitted by the Author:	10-Feb-2015
Complete List of Authors:	Zhang, Xi; University of Wisconsin-Madison, Department of Electrical & Computer Engineering Liu, Hewei; University of Wisconsin-Madison, Department of Electrical & Computer Engineering Huang, Xuezhen; University of Wisconsin-Madison, Electrical and Computer Engineering Jiang, Hongrui; University of Wisconsin - Madison, Electrical and Computer Engineering

Cite this: DOI: 10.1039/c0xx00000x

Paper

www.rsc.org/xxxxxx

## One-step femtosecond laser patterning of light-trapping structure on dye-sensitized solar cell photoelectrode

Xi Zhang,<sup>‡</sup> Hewei Liu,<sup>‡</sup> Xuezheng Huang<sup>a</sup> and Hongrui Jiang<sup>\*a</sup>

Received (in XXX, XXX) Xth XXXXXXXXX 20XX, Accepted Xth XXXXXXXXX 20XX

DOI: 10.1039/b000000x

Light-trapping patterns were constructed in TiO<sub>2</sub> photoelectrodes for dye-sensitized solar cells (DSSCs) by a one-step femtosecond laser structuring method that utilized ablation to create patterns at the surface of nanostructured TiO<sub>2</sub> films. As a result, much more light was trapped in the photoelectrodes. Grating and orthogonal-grid patterns were studied, and the light trapping performance was optimized through the adjustment of pattern spacing, which was easily realized in the laser ablation process. With a 5- $\mu$ m-spacing orthogonal-grid pattern, DSSCs showed a highest photon-to-electron conversion efficiency of 9.32% under AM 1.5G, a 13.5% improvement compared to the same cell without laser ablation. This simple and universal laser ablation method could be used to process many kinds of nanomaterials, and could be applied for various devices with nanostructures.

### 1. Introduction

Light-trapping designs and structures inside solar cells can overcome the insufficient light harvesting of the absorbing layers owing to their limited thickness. Therefore they are effective in improving the photon-to-electron conversion efficiency ( $\eta$ ), and have been extensively studied in recent years for different types of solar cells.<sup>1-6</sup> The light-trapping structures are generally patterned on the photoactive layers. Dye-sensitized solar cell (DSSC) is considered as a promising type of solar cell due to its low cost and high efficiency.<sup>7-9</sup> The research on enhancing the light absorption of DSSCs is thus always a topic of great interest. The introduction of large TiO<sub>2</sub> nanoparticles as scattering centers in the photoelectrode is a conventional method to improve the light absorption.<sup>10,11</sup> Other methods exist too, such as taking advantage of the plasmonic effect,<sup>12-14</sup> modifying the electrolyte,<sup>15</sup> and using photonic crystals.<sup>16</sup> Creating light-trapping structures in DSSCs via patterning could be more efficient.<sup>17-21</sup> However, different from conventional solar cells based on bulk materials, patterning on nanostructured TiO<sub>2</sub> for DSSCs is much more difficult. So far, there has been only one method, which is essentially through template molding, applied for the DSSCs based on printed TiO<sub>2</sub> photoelectrode. Kim *et al.* first reported nanopatterned TiO<sub>2</sub> photoelectrode for DSSCs via a polydimethylsiloxane (PDMS) nanostamp.<sup>19</sup> Wooh *et al.* fabricated pyramid-like structures via pressing a mold onto the top of a TiO<sub>2</sub> paste, and obtained high performance of the DSSCs.<sup>20</sup> Recently, Lee *et al.* patterned a grating structure on the bottom of TiO<sub>2</sub> photoelectrode using a PDMS stamp.<sup>21</sup> Nevertheless, this method requires that the electrode materials be in paste-like state for printing before solidification. It would be advantageous if the solidified TiO<sub>2</sub> photoelectrode could be

directly patterned, eliminating the requirement on the state of the electrode material. There has been no report yet, though, on such one-step patterning on the nanostructured TiO<sub>2</sub> photoelectrode.

Femtosecond (fs) laser ablation has been proven a simple and effective method to create micro- or nano-structures directly onto the surface of bulk materials.<sup>22-26</sup> In this study, we utilized fs laser to directly ablate the surface of nanostructured TiO<sub>2</sub> film and obtain a periodic morphology for light-trapping. This one-step fabrication utilizing fs laser ablation is a cost-effective, versatile and environmentally friendly approach, and can form any patterns without photolithography and its intrinsically involved steps. More importantly, this universal method can be applied to many more categories of nanomaterials, and is not limited by the fabrication process of the devices or the states of the materials during the process. The sub-picosecond laser-matter interaction avoids thermal damages of the materials and substrates, and allows for fabrication of structures within a few micrometers.<sup>27</sup> The fs laser generates hierarchical structures combining both micro- and nano-scales in a single ablation<sup>28,29</sup>; such dual-scale micro-/nano-structure can increase the surface area of TiO<sub>2</sub>.

A grating pattern and an orthogonal-grid pattern were adopted in this work and various size parameters of the patterns were investigated. The laser-ablated TiO<sub>2</sub> photoelectrode with 5- $\mu$ m orthogonal-grid spacing demonstrated the strongest light-trapping effect. The corresponding fabricated DSSCs showed the highest  $\eta$  of 9.32%, increased from 8.21% without laser ablation, indicating a 13.5% of improvement in  $\eta$  due to laser patterning of TiO<sub>2</sub> photoelectrode alone. This universal laser ablation method also has great potential for other types of nanostructured solar cells.

### 2. Experimental

10- $\mu\text{m}$ -thick  $\text{TiO}_2$  film consisting of 20-nm  $\text{TiO}_2$  nanoparticles was deposited onto fluorine-doped tin oxide (FTO) glass (1.5 cm  $\times$  1.5 cm, TEC-15, MTI Co.) using a screen-printing method before being sintered at 500  $^\circ\text{C}$ . The area of the active region on the FTO glass was 0.12  $\text{cm}^2$ , measured by a microscope (Olympus BX51M).

The vertical-polarized laser (Uranus2000-1030-1000, PolarOnyx) with pulse duration of 700 fs, wavelength of 1030 nm, and repetition rate of 120 kHz were delivered into an objective lens (N.A. = 0.8, Nikon) and focused on the sample surface. The diameter of the focal spot was 1.5  $\mu\text{m}$ . A mechanical shutter was used to turn the laser on and off. A neutral density attenuator and polarizer were used to control the power and polarization of the laser beam. The sample was mounted on a computer-controlled  $xyz$  stage (Newport XMS-160, XMS-100 and GTS-30V for the  $x$ -axis,  $y$ -axis and  $z$ -axis, respectively). By translating the sample, the microstructures were ablated by the focused laser pulses, and a CCD camera and relay lens were used for real-time monitoring of the ablation process. The laser energy was 40 nJ per pulse, and the scanning speed was 2 mm/s.

The ablated  $\text{TiO}_2$  films with grating and orthogonal-grid patterns were then cleaned with deionized water before being coated with a 3- $\mu\text{m}$ -thick scattering layer consisting of 50-nm  $\text{TiO}_2$  nanoparticles using the same screen-printing method. The films were subsequently sintered again at 500  $^\circ\text{C}$  for 1 h. After being cooled down to 120  $^\circ\text{C}$ , they were soaked into the dye solutions (0.3 mM N719 in acetonitrile-tert-butanol,  $v/v = 1 : 1$ ) and kept at room temperature for 24 h. The counter electrode was Pt-coated FTO glass with two drilled holes for filling the electrolyte. The Pt layer was deposited onto the FTO glass by an electrodeposition process in  $\text{H}_2\text{PtCl}_6$  solution (0.5 M). A 25- $\mu\text{m}$ -thick Surlyn (SOLARONIX, Switzerland) film was used as a spacer between the photoelectrode and the counter electrode for each DSSC. The redox electrolyte contained 0.1 M LiI, 0.05 M  $\text{I}_2$ , and 0.6 M 1,2-dimethyl-3-propylimidazolium iodide, using acetonitrile as solvent.

The morphology of the  $\text{TiO}_2$  film surfaces were characterized by scanning electron microscopy (SEM, Zeiss LEO 1530). X-ray diffraction (XRD) spectra of  $\text{TiO}_2$  films were measured by a Bruker/Siemens Hi-Star 2d X-ray diffractometer with a monochromatic Cu K-alpha point source (0.8 mm). The optical transmittance and reflectance spectra of the  $\text{TiO}_2$  photoelectrodes were measured by an optical fiber detector (Edmund) equipped with an integrating sphere (Thorlabs). The  $J$ - $V$  measurements of the DSSCs were performed using a Keithley 2400 source meter under the illumination of simulated AM 1.5G solar light (Oriel 94022A equipped with a 150W Xe lamp and an AM 1.5G filter). For the incident photon-to-current efficiency (IPCE) measurement,  $J_{\text{sc}}$  of DSSCs at each wavelength in the range of 400 – 700 nm was recorded by the Keithley 2400 source meter before the IPCE values were calculated. The light from the Oriel 94022A light source was conducted through a monochromator (Mini-Chrom 300 – 800 nm, Edmund Optics) and illuminated to the DSSCs. The wavelength step was set to 10 nm. The amount of adsorbed dye was determined from the absorbance of the desorbed dye solution at 510 nm using the same monochromator. The dye-loaded  $\text{TiO}_2$  films were immersed in 0.1 M NaOH aqueous solution for 20 min for dye desorption.

The transmittance spectra of the  $\text{TiO}_2$  photoelectrodes with and without laser ablation were simulated by the software Zemax (Radiant Zemax).

### 3. Results and Discussion

#### 3.1. Patterning by Laser Ablation

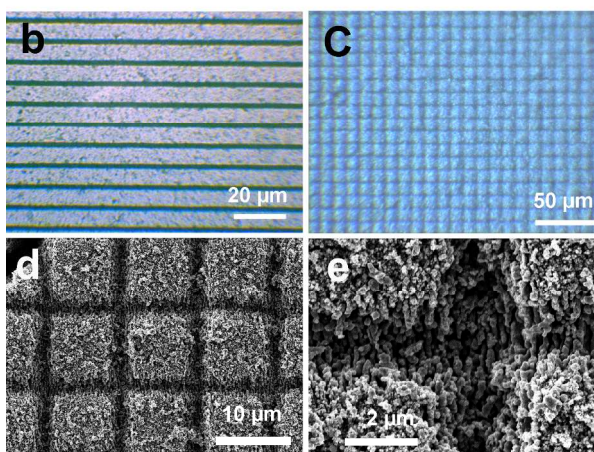
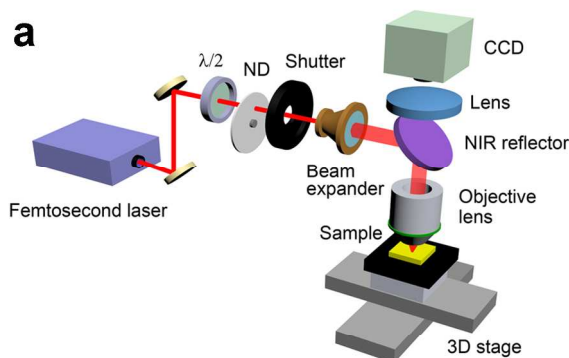


**Fig. 1** (a) Schematic of the optical setup for the laser ablation structuring; (b) a grating pattern (10- $\mu\text{m}$  grid spacing) of the laser-ablated nanostructured  $\text{TiO}_2$  film; (c) an orthogonal-grid pattern (10- $\mu\text{m}$  grid spacing) of the laser-ablated nanostructured  $\text{TiO}_2$  film; (d) SEM image of the orthogonal-grid pattern; (e) enlarged image of (d): the formation of the nanostructures in the laser irradiated regions.

The optical setup for structuring the  $\text{TiO}_2$  thin film is shown in Fig. 1a. Linear polarized laser pulses were delivered into an objective lens and focused on the sample surface. A nanostructured  $\text{TiO}_2$  photoelectrode before laser ablation was deposited onto a FTO glass substrate, followed by sintering at 500  $^\circ\text{C}$ . The thickness of the  $\text{TiO}_2$  film was 10  $\mu\text{m}$ , consisting of 20-nm nanoparticles. By scanning the laser beam along programmed paths, any pattern could be directly written onto the  $\text{TiO}_2$  film without other processing. The pulse width was 700 fs, which is much shorter than the heat diffusion time between the lattice of  $\text{TiO}_2$ . Hence the thermal effect could hardly affect the porosity of the nanostructure  $\text{TiO}_2$  film.<sup>30</sup> In the experiments, both grating and orthogonal-grid patterns were defined. The optical microscopic images of a grating and an orthogonal-grid pattern are shown in Fig. 1b and c, respectively. Both the grating and orthogonal-grid patterns had intervals between two grid lines

ranging between 5  $\mu\text{m}$  and 40  $\mu\text{m}$ . The detail of the structures is shown in the SEM image (Fig. 1d). The line width of the grids was about 2  $\mu\text{m}$ , while the ablation depth was also about 2  $\mu\text{m}$ . An interesting phenomenon is the formation of nanostructures in the laser irradiated regions, as shown in Fig. 1e. These structures can be categorized as the laser-induced periodic surface structures that were commonly observed after laser ablation and that were demonstrated to increase the surface area of the material.<sup>28,29</sup>

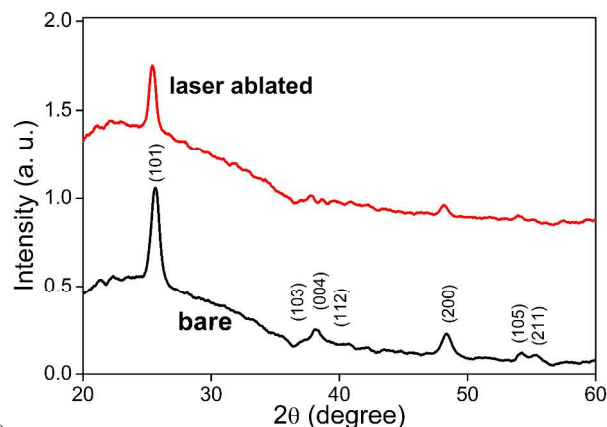


Fig. 2 XRD spectra of nanostructured  $\text{TiO}_2$  film before and after laser ablation.

XRD measurements were performed to explore the potential change in  $\text{TiO}_2$  induced by the laser ablation. Fig. 2 shows the XRD spectra of the  $\text{TiO}_2$  film before and after laser ablation. All the peaks in the spectrum of the bare  $\text{TiO}_2$  film are indexed to standard anatase pattern. After laser ablation, the positions of all the peaks did not change and no extra peaks were observed. Therefore, the lattice of anatase  $\text{TiO}_2$  nanoparticles was not modified by the laser ablation process, nor was any impurity or contamination introduced.

### 3.2. Light-trapping Effect

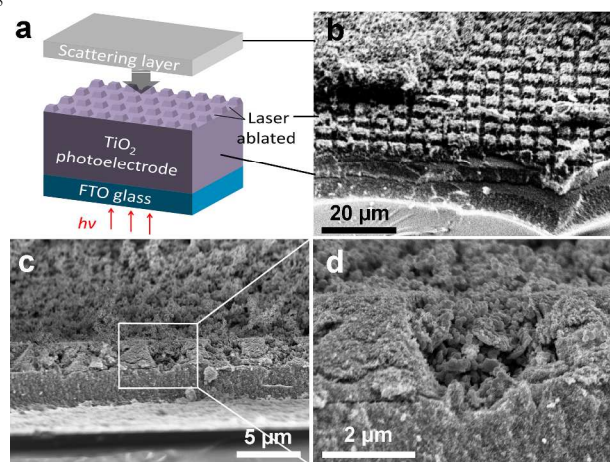


Fig. 3 (a) Schematic of  $\text{TiO}_2$  photoelectrode, which is patterned by laser ablation and covered by a scattering layer; (b), (c) cross-sectional SEM images of the  $\text{TiO}_2$  film with an orthogonal-grid structure (5- $\mu\text{m}$  grid spacing) covered by the scattering layer; (d) enlarged image of the selected region in (c).

After laser ablation, the 10- $\mu\text{m}$ -thick  $\text{TiO}_2$  film was covered with a 3- $\mu\text{m}$ -thick scattering layer, which consisted of 50-nm  $\text{TiO}_2$  particles. Fig. 3 shows the cross-sectional SEM images of the  $\text{TiO}_2$  film with the orthogonal-grid structure covered by the scattering layer. The laser-ablated lines show sloped sidewalls with a height of 2  $\mu\text{m}$ . Such sloped sidewalls benefit the reflection of light, thus the light trapping effect.<sup>20</sup> The cross-sectional profile and the depth of the laser-ablated structures can be changed by varying the focusing condition, the power, and the scanning speed of the laser.

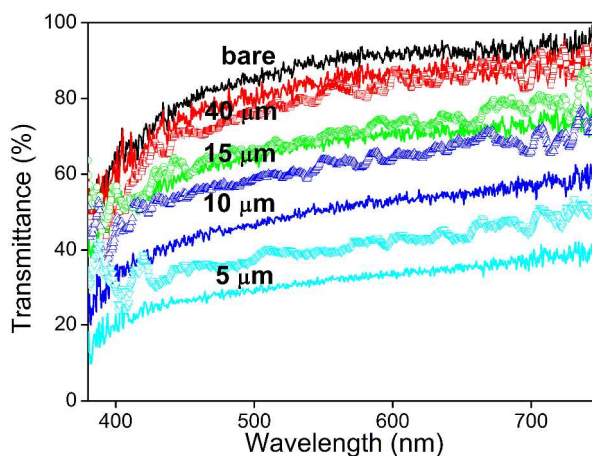
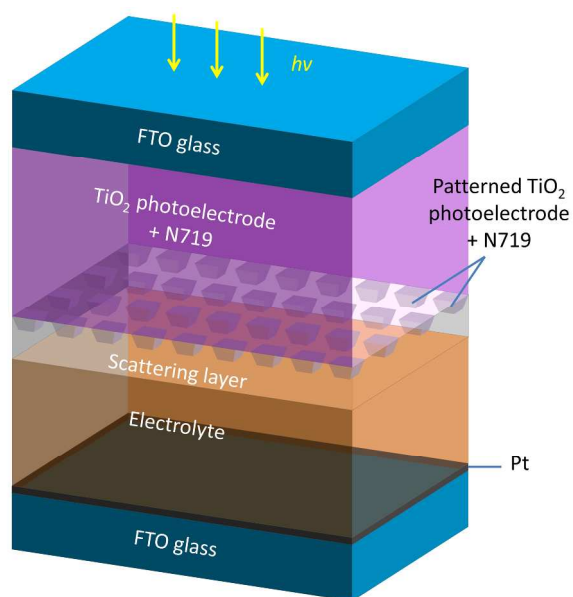


Fig. 4 Transmittance spectra of nanostructured  $\text{TiO}_2$  films before and after laser ablation. The grid spacings of both the grating and the orthogonal-grid patterns on the ablated photoelectrodes are 5  $\mu\text{m}$  (light blue curves), 10  $\mu\text{m}$  (blue curves), 15  $\mu\text{m}$  (green curves), and 40  $\mu\text{m}$  (red curves), respectively. The black solid curve indicates the bare film. The colored solid curves indicate the films with the orthogonal-grid patterns. The colored scatter curves indicate the films with the grating patterns.

In this study, four grid spacings of 5  $\mu\text{m}$ , 10  $\mu\text{m}$ , 15  $\mu\text{m}$ , and 40  $\mu\text{m}$  were used for both the grating and the orthogonal-grid patterns. In order to observe the effect of light-trapping by laser ablation, the transmittance spectra of the  $\text{TiO}_2$  films without the scattering layer were measured. Fig. 4 shows the results of the bare and the laser-ablated  $\text{TiO}_2$  films with the same thickness of 10  $\mu\text{m}$ . The reduced light transmittance after laser ablation indicates the enhanced light reflection plus absorption from the significantly increased surface area on top of the  $\text{TiO}_2$  photoactive layer by laser ablation, which benefits the light harvesting of DSSCs. For each grid spacing, the grating pattern has a higher transmittance than that of the orthogonal-grid pattern, because the latter has a nearly doubled ablation area. As the grid spacing decreases, the reflected and scattered light increases owing to the increased density of the light trapping structure. Therefore, the transmittance decreases gradually. From Fig. 4, there was little reduction in transmittance when the grid spacing reached 40  $\mu\text{m}$ . The reflectance spectra of the bare and laser-ablated  $\text{TiO}_2$  films are shown in Fig. S1 (ESI †), where the reflectance is increased after laser ablation, and the orthogonal-grid pattern has a higher reflectance than that of the grating pattern. Fig. S2 (ESI †) shows the simulated transmittance spectra of the orthogonal-grid patterns, which are in agreement with the measured results.

### 3.3. Performance of DSSCs



**Fig. 5** Schematic of the DSSC with patterned TiO<sub>2</sub> photoelectrode by laser ablation.

After being covered with 3- $\mu\text{m}$ -thick scattering layers, the bare and laser-ablated TiO<sub>2</sub> films were loaded with dyes before assembled into DSSCs. The schematic of a final DSSC with an orthogonal-grid-patterned TiO<sub>2</sub> photoelectrode is shown in Fig. 5. The  $J$ - $V$  results of all these DSSCs under simulated AM 1.5G illumination are shown in Fig. 6, and all the corresponding parameters are listed in Table 1. For the DSSCs with laser ablation, the grid spacings for each of the two patterns were also 5  $\mu\text{m}$ , 10  $\mu\text{m}$ , 15  $\mu\text{m}$ , and 40  $\mu\text{m}$  respectively. The width of laser-ablated line was kept the same at 2  $\mu\text{m}$ .  $\eta$  of the DSSC without laser ablation was 8.21%. The short-circuit photocurrent density ( $J_{\text{sc}}$ ) was significantly improved after the photoelectrode was laser-ablated with the light-trapping grids, while the open-circuit voltage ( $V_{\text{oc}}$ ) remained at about 0.7 V. The fill factor (FF) was reduced a little after laser ablation, but remained at almost the same level for different pattern parameters.  $\eta$  for the four DSSCs with grating patterns ranges from 8.61% to 9.14%, while  $\eta$  for the four DSSCs with orthogonal-grid patterns ranges from 9.16% to 9.32%, all of which are much higher in comparison with the cell without laser ablation. This indicates that the patterned light-trapping grids on the photoelectrode improve the light scattering effect, which in turn enhances the total light absorption of the cell. As mentioned before, the ablation depth was about 2  $\mu\text{m}$ , which removed a small portion of the total 10- $\mu\text{m}$ -thick dye-loaded TiO<sub>2</sub> layer. The laser ablation has a quite limited influence on the amount of the loaded dye molecules, and would not increase the dye amount. The measured amount of adsorbed dye on each TiO<sub>2</sub> films is shown in Table S1 (ESI †). The dye amount was reduced after laser ablation. Therefore, the performance enhancement is ascribed to the light-trapping effect. The improvement of  $\eta$  is mainly attributed to the enhancement of  $J_{\text{sc}}$ .

For either the grating pattern or the orthogonal-grid pattern with 40 different spacings, the performance of DSSCs increases as the spacing decreases. As expected, the DSSC with the orthogonal-grid pattern has a better performance than that with the grating pattern at each given grid spacing. For both types of patterns,  $J_{\text{sc}}$  is significantly improved from no ablation to 40  $\mu\text{m}$  of spacing and then down to 15  $\mu\text{m}$  of spacing. However,  $J_{\text{sc}}$  remains almost at the same level from 15  $\mu\text{m}$  of spacing to 5  $\mu\text{m}$  of spacing for both types of patterns, although the transmittance kept decreasing as shown in Fig. 4. This implies that not all of the increased trapped light contributed to the ultimate photocurrent generation.

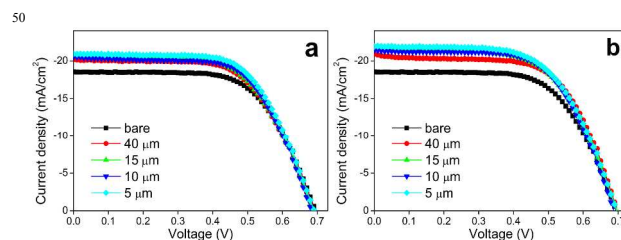


**Fig. 6**  $J$ - $V$  curves of the DSSCs using bare and laser-ablated TiO<sub>2</sub> photoelectrodes. (a) DSSCs with bare and grating-patterned TiO<sub>2</sub>; (b) DSSCs with bare and orthogonal-grid-patterned TiO<sub>2</sub>. The grid spacing of both types of patterns on the ablated photoelectrodes ranges from 5  $\mu\text{m}$  to 40  $\mu\text{m}$ .

**Table 1.**  $J$ - $V$  parameters of all the DSSCs.

Pattern	$V_{\text{oc}}$ (V)	$J_{\text{sc}}$ (mA/cm <sup>2</sup> )	FF (%)	$\eta$ (%)
bare	0.70	18.6	63.2	8.21
40 $\mu\text{m}$ grating	0.69	20.2	61.8	8.61
15 $\mu\text{m}$ grating	0.69	20.6	61.3	8.73
10 $\mu\text{m}$ grating	0.69	20.5	62.7	8.88
5 $\mu\text{m}$ grating	0.70	20.9	62.4	9.14
40 $\mu\text{m}$ orthogonal	0.70	20.9	62.6	9.16
15 $\mu\text{m}$ orthogonal	0.70	21.9	60.0	9.18
10 $\mu\text{m}$ orthogonal	0.69	21.6	61.8	9.23
5 $\mu\text{m}$ orthogonal	0.70	21.9	60.7	9.32

The results of the IPCE measurements from 400 nm to 750 nm are shown in Fig. 7. For each of the two pattern types, the IPCE increases as the grid spacing decreases in the full range, which agrees well with the trend in  $J_{\text{sc}}$ . The IPCE improvement after the formation of the light-trapping structure covers almost all wavelengths measured. For the curves corresponding to 10  $\mu\text{m}$ , 15  $\mu\text{m}$ , 40  $\mu\text{m}$  of spacing in Fig. 7a and 40  $\mu\text{m}$  of spacing in Fig. 7b, the increase mainly lies in the wavelength range below 600 nm, which is quite different from the transmittance results in Fig. 4, where the increase almost covers the whole wavelength range. This indicates that the trapped light by the ablated patterns has a wavelength selectivity when absorbed by the dye. One of the reasons could be the dependence of reflection angle on

wavelength. When the grid spacing of the grating pattern is reduced to 5  $\mu\text{m}$  or the grid spacing of the orthogonal-grid pattern is reduced to 15  $\mu\text{m}$  and less, the increase in IPCE above 600 nm becomes more significant. For the orthogonal-grid patterns, the IPCEs of the DSSCs with 5- $\mu\text{m}$ , 10- $\mu\text{m}$ , and 15- $\mu\text{m}$  spacings are much greater than that with 40- $\mu\text{m}$  spacing. This agrees with the variation in  $J_{\text{sc}}$  with the same spacings. The ablated surface reflected more light back to the dye-loaded photoelectrode, and the photocurrent increased. The parameters of the laser-ablated pattern could influence the scattering of the light at different wavelengths, and a better matching with the absorption spectrum of the dye could result in better performance of DSSCs.

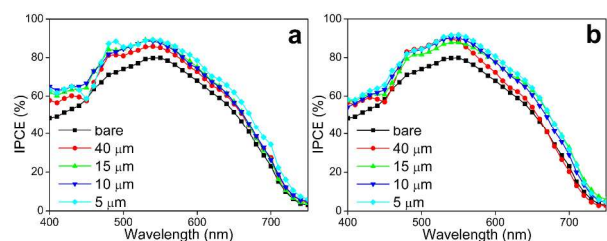


**Fig. 7** IPCE spectra of the DSSCs using bare and laser-ablated  $\text{TiO}_2$  photoelectrodes. (a) DSSCs with bare and grating-patterned  $\text{TiO}_2$ ; (b) DSSCs with bare and orthogonal-grid-patterned  $\text{TiO}_2$ . The grid spacing of both types of patterns on the ablated photoelectrodes ranges from 5  $\mu\text{m}$  to 40  $\mu\text{m}$ .

## Conclusions

In conclusion, we utilized fs laser ablation to directly write grating and orthogonal-grid patterns as light-trapping structures on nanostructured  $\text{TiO}_2$  films to enhance light harvesting in DSSCs. The fabricated DSSCs with the light-trapping structures on the photoelectrodes showed significantly improved performance. The parameters of the patterns could be easily adjusted in the laser ablation process. The grid spacing was varied to optimize the light trapping effect. The  $\text{TiO}_2$  film with 5- $\mu\text{m}$  orthogonal-grid spacing demonstrated the best light-trapping effect, and the corresponding DSSC presented the highest  $\eta$  of 9.32%, which is a 13.5% improvement compared with the DSSC without laser ablation. This simple, single-step fs laser ablation process is universal and can be applied to processing of many kinds of nanomaterials for a host of applications. For example, it could be utilized to improve the light harvesting efficiency of a number of novel solar cells based on nanostructures. Another example would be the production of novel optical materials taking advantage of the dual-scale micro-/nano-structures. In the future, the wavelength selectivity of the patterns by laser ablation will be further investigated, and the detailed light-trapping mechanism will be explored.

## Acknowledgements

This work was supported by the US National Institute of Health (Grant No. 1DP2OD008678-01). This research utilized NSF supported shared facilities at the University of Wisconsin.

## Notes and References

<sup>a</sup> Materials Science Program, Department of Electrical and Computer Engineering, University of Wisconsin-Madison, Madison, WI, 53706.

USA. Fax: 608-262-1267; Tel: 608-265-9418. E-mail:

hongrui@engr.wisc.edu

<sup>†</sup> Electronic Supplementary Information (ESI) available. See DOI: 10.1039/b000000x/

<sup>‡</sup> X. Zhang and H. Liu contributed equally to this work.

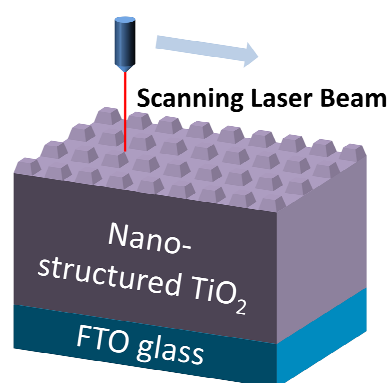
- E. Garnett, P. Yang, *Nano Lett.* **2010**, 10, 1082.
- H. A. Atwater, A. Polman, *Nat. Mater.* **2010**, 9, 205.
- C. Battaglia, J. Escarré, K. Söderström, L. Erni, L. Ding, G. Bugnon, A. Billet, M. Boccard, L. Barraud, S. D. Wolf, F.-J. Haug, M. Despeisse, C. Ballif, *Nano Lett.* **2011**, 11, 661.
- C. Battaglia, J. Escarré, K. Söderström, M. Charrière, F.-J. Haug, M. Despeisse, C. Ballif, *Nat. Photonics* **2011**, 5, 535.
- D. M. Callahan, J. N. Munday, H. A. Atwater, *Nano Lett.* **2012**, 12, 214.
- R. Betancur, P. Romero-Gomez, A. Martinez-Otero, X. Elias, M. Maymo, J. Martorell, *Nature Photonics* **2013**, 7, 995.
- M. Grätzel, R. A. J. Janssen, D. B. Mitzi, E. H. Sargent, *Nature* **2012**, 488, 304.
- B. E. Hardin, H. J. Snaith, M. D. McGehee, *Nat. Photonics* **2012**, 6, 162.
- A. Yella, H. W. Lee, H. N. Tsao, C. Y. Yi, A. K. Chandiran, Md. K. Nazeeruddin, E. W. G. Diau, C. Y. Yeh, S. M. Zakeeruddin, M. Grätzel, *Science* **2011**, 334, 629.
- S. Hore, C. Vetter, R. Kern, H. Smit, A. Hinsch, *Sol. Energy Mater. Sol. Cells* **2006**, 90, 1176.
- F. Huang, D. Chen, X. L. Zhang, R. A. Caruso, Y.-B. Cheng, *Adv. Funct. Mater.* **2010**, 20, 1301.
- S. Guldin, S. Hüttner, M. Kolle, M. E. Welland, P. Müller-Buschbaum, R. H. Friend, U. Steiner, N. Tétreault, *Nano Lett.* **2010**, 10, 2303.
- A. Mihi, C. Zhang, P. V. Braun, *Angew. Chem. Int. Ed.* **2011**, 50, 5712.
- C. T. Yip, H. Huang, L. Zhou, K. Xie, Y. Wang, T. Feng, J. Li, W. Y. Tam, *Adv. Mater.* **2011**, 23, 5624.
- M. Wang, X. Pan, X. Fang, L. Guo, W. Liu, C. Zhang, Y. Huang, L. Hu, S. Dai, *Adv. Mater.* **2010**, 22, 5526.
- I.-K. Ding, J. Zhu, W. Cai, S.-J. Moon, N. Cai, P. Wang, S. M. Zakeeruddin, M. Grätzel, M. L. Brongersma, Y. Cui, M. D. McGehee, *Adv. Eng. Mater.* **2011**, 1, 52.
- F. Wang, N. K. Subbaiyan, Q. Wang, C. Rochford, G. Xu, R. Lu, A. Elliot, F. D'Souza, R. Hui, J. Wu, *ACS Appl. Mater. Interfaces* **2012**, 4, 1565.
- J.-H. Kim, D.-H. Kim, K.-P. Kim, D.-H. Jeon, D.-K. Hwang, *Thin Solid Films* **2013**, 546, 326.
- J. Kim, J. K. Koh, B. Kim, J. H. Kim, E. Kim, *Angew. Chem. Int. Ed.* **2012**, 51, 6864.
- S. Wooh, H. Yoon, J.-H. Jung, Y.-G. Lee, J. H. Koh, B. Lee, Y. S. Kang, K. Char, *Adv. Mater.* **2013**, 25, 3111.
- J. Lee, M. Lee, *Adv. Energy Mater.* **2014**, 4, 1300978.
- Y. Shimotsuma, P. G. Kazansky, J. Qiu, K. Hirao, *Phys. Rev. Lett.* **2003**, 91, 247405.
- A. P. Joglekar, H. Liu, E. Meyhofer, G. Mourou, A. J. Hunt, *PNAS* **2004**, 101, 5856.
- M. Shen, J. E. Carey, C. H. Crouch, M. Kandyla, H. A. Stone, E. Mazur, *Nano Lett.* **2008**, 8, 2087.
- M. Farsari, B. N. Chichkov, *Nat. Photonics* **2009**, 3, 450.
- U. Zywiets, A. B. Evlyukhin, C. Reinhardt, B. N. Chichkov, *Nat. Commun.* **2014**, 5, 3402.
- R. R. Gattass, E. Mazur, *Nat. Photonics* **2008**, 2, 219.
- M. Huang, F. Zhao, Y. Cheng, N. Xu, Z. Xu, *ACS Nano* **2009**, 3, 4062.
- V. R. Bhardwaj, E. Simova, P. P. Rajeev, C. Hnatovsky, R. S. Taylor, D. M. Rayner, P. B. Corkum, *Phys. Rev. Lett.* **2006**, 96, 057404.
- J. Yoon, M. Jin, M. Lee, *Adv. Mater.* **2011**, 23, 3974.

## Table of Content

### One-step femtosecond laser patterning of light-trapping structure on dye-sensitized solar cell photoelectrode

<sup>5</sup> Xi Zhang, Hwei Liu, Xuezheng Huang, and Hongrui Jiang\*

[\*] Prof. H. Jiang, Dr. X. Zhang, Dr. H. Liu, Dr. X. Huang  
Materials Science Program, Department of Electrical and Computer Engineering  
University of Wisconsin-Madison  
<sup>10</sup> Madison, WI 53706 (USA)  
E-mail: hongrui@engr.wisc.edu



<sup>15</sup> Light-trapping patterns constructed in TiO<sub>2</sub> photoelectrodes by femtosecond laser ablation improve efficiency of dye-sensitized solar cells by up to 13.5%.